

# **UNIVERSIDAD SAN FRANCISCO DE QUITO USFQ**

**Colegio de Ciencias e Ingeniería**

## **Sound Visualization with an Acoustic Camera**

**Lino Moisés Mediavilla Ponce**

**Ingeniería Mecánica**

Trabajo de integración curricular presentado como requisito  
para la obtención del título de  
Ingeniero Mecánico

Quito, 16 de diciembre de 2019

UNIVERSIDAD SAN FRANCISCO DE QUITO USFQ  
COLEGIO DE CIENCIAS E INGENIERÍA

**HOJA DE CALIFICACIÓN  
DE TRABAJO DE INTEGRACIÓN CURRICULAR**

**Sound Visualization with an Acoustic Camera**

**Lino Moisés Mediavilla Ponce**

**Calificación:**

/

**Nombre del profesor, Título académico**

**Patricio Chiriboga , Ph.D**

**Nombre del profesor, Título académico**

**Alfredo Valarezo , Ph.D**

**Firma del profesor:**

\_\_\_\_\_

Quito, 16 de diciembre de 2019

## Derechos de Autor

Por medio del presente documento certifico que he leído todas las Políticas y Manuales de la Universidad San Francisco de Quito USFQ, incluyendo la Política de Propiedad Intelectual USFQ, y estoy de acuerdo con su contenido, por lo que los derechos de propiedad intelectual del presente trabajo quedan sujetos a lo dispuesto en esas Políticas.

Asimismo, autorizo a la USFQ para que realice la digitalización y publicación de este trabajo en el repositorio virtual, de conformidad a lo dispuesto en el Art. 144 de la Ley Orgánica de Educación Superior.

Firma del estudiante:

---

Nombres y apellidos:

Lino Moisés Mediavilla Ponce

Código:

00115753

Cédula de identidad:

1311645186

Lugar y fecha:

Quito, 16 de diciembre de 2019

## RESUMEN

Hoy en día, para la caracterización de fuentes de sonido se emplean cámaras acústicas, que permiten obtener mapas de intensidad sobrepuestos en imágenes digitales de escenarios analizados. Este trabajo explica el proceso de construir tal dispositivo, desde el diseño del arreglo de micrófonos hasta la integración de las capas de software requeridas. Una tarjeta de adquisición de datos National Instruments y el software LabView se usaron para registrar las señales de un arreglo de 16 micrófonos omnidireccionales de manera simultánea, mientras que la librería de código abierto Acoular.py se usó para procesarlas, aplicando técnicas de Beamforming. Como resultado se obtuvo un prototipo de cámara acústica capaz de distinguir y caracterizar fuentes de sonido estáticas en un rango de frecuencias entre 2.8 kHz y 6 kHz.

*Palabras clave:* Arreglo de micrófonos, Beamforming, Cámara Acústica, Python.

## ABSTRACT

Nowadays, characterization of sound sources is being carried out with acoustic cameras, which allow to obtain entire sound intensity maps overlaid on digital images of the scenarios under study at once, as opposed to individual sound probes. This work explains the process of building such a device, from the design of the microphone array to the integration of the required software layers. A National Instruments data acquisition card and LabView were used to record the signals of an array of 16 condenser microphones simultaneously, while the open source library Acoular.py was used to process the signals, applying beamforming techniques. The result was a prototype of an acoustic camera capable of distinguishing and characterizing static sound sources in a frequency range from 2.8 kHz up to 6 kHz.

**Keywords:** *Microphone Array, Beamforming, Acoustic Camera, Python.*

## CONTENT TABLE

<b>INTRODUCTION .....</b>	<b>9</b>
<b>METHODOLOGY .....</b>	<b>11</b>
<b>Array Signal Processing .....</b>	<b>11</b>
<b>Microphone Array Design .....</b>	<b>13</b>
F Parameter.....	16
Simulations.....	16
<b>Hardware and Software components .....</b>	<b>20</b>
Sensors .....	20
Processing.....	20
User interface .....	21
<b>RESULTS .....</b>	<b>23</b>
<b>Test set 1 .....</b>	<b>23</b>
<b>Test set 2 .....</b>	<b>27</b>
<b>Test set 3 .....</b>	<b>29</b>
<b>DISCUSSION .....</b>	<b>31</b>
<b>CONCLUSIONS .....</b>	<b>34</b>
<b>REFERENCES .....</b>	<b>35</b>
<b>APPENDIX A: Layout and exact microphone positions in the acoustic camera prototype .....</b>	<b>37</b>
<b>APPENDIX B: Circuit schematic for the microphone power supply stage .....</b>	<b>38</b>
<b>APPENDIX C: Circuit schematic for the microphone pre-amplification stage.....</b>	<b>38</b>

**TABLE INDEX**

Table 1. Location and strength of three synthetic point sources with respect to the center of the array.....	17
Table 2. Localization and intensity errors (single sound source test, at 0.5 m from the array). .....	32

## FIGURE INDEX

Figure 1. Working principle of beamforming.....	12
Figure 2. Underbrink spiral microphone array distribution.....	15
Figure 3. Acoustic map of three arbitrary point sources (3 kHz third-octave band, 16- microphone underbrink spiral array).....	18
Figure 4. Acoustic map of three arbitrary point sources (10 kHz third-octave band, 64- microphone Underbrink spiral array).....	19
Figure 5. Acoustic map of three arbitrary point sources (10 kHz third-octave band, 16- microphone Underbrink spiral array).....	19
Figure # 6. Acoustic camera prototype built for this project. ....	22
Figure # 7. Sound source set-up for test set # 1 .....	23
Figure # 8. Resulting acoustic maps for test set 1, at 0.3 m.....	24
Figure # 9. Resulting acoustic maps for test set 1, at 0.5 m.....	25
Figure # 10. Resulting acoustic maps for test set 1, at 0.8 m. (Frequency range extended due to attenuations experienced in lower frequencies). ....	26
Figure # 11. Sound source set-up for test set # 2 .....	27
Figure # 12. Resulting acoustic maps for test set 2.....	28
Figure # 13. Sound source set-up for test set # 3 .....	29
Figure # 14. Resulting acoustic map for test set # 3, from 3 kHz to 6 kHz.....	29
Figure # 15. Resulting acoustic map for test set # 3, from 3.9 kHz to 4.1 kHz.....	30
Figure # 16. Resulting acoustic map for test set # 3, from 5 kHz to 6 kHz.....	30



## INTRODUCTION

Generation of acoustic maps is of great interest in the areas of vehicle design (Döbler & Heilmann, 2015), low-noise machinery design (Sarradj & Herold, 2017), machinery diagnosis (Orman, Rzeszucinski, & Pinto, 2014), 3D surface generation (Legg & Bradley, 2014) and architecture (Ortiz, Barré, & Vorrhein, 2015).

These maps can be obtained using acoustic cameras, which are devices that sample sound sources through a microphone array and compute acoustic maps from which “location, strength, and spectrum of the sources can be estimated” (Sarradj & Herold, 2017). Additionally, these maps can be overlaid on top of digital images of the objects or spaces being studied, allowing for a more straightforward interpretation of results.

Although some companies around the globe are already producing acoustic cameras (Aldeman & Raman, 2018) and offering consulting services, their software is either hardware-bound or closed-source (Sarradj & Herold, 2017). In reaction to this, Sarradj & Herold developed the open-source library Acoular. This contains implementations of several algorithms for microphone array signal processing, and key optimizations for performance like result caching, and parallelization (Sarradj & Herold, 2017). The use of this library for either research or production environments has been encouraged by its authors.

The aim of this work is to produce a working prototype of an acoustic camera that is capable of distinguishing and characterizing static sound sources, by producing two-dimensional acoustic maps overlaid on top of digital images of the studied scenarios, making use of the open source Acoular library and providing a user-friendly interface.

The rest of this work is organized as follows: first a brief background of microphone array signal processing methods is presented, then the details underlying the physical design of the microphone array are discussed. Next, the required hardware and software components for data acquisition, processing and result visualization are described. Afterwards, the results of

benchmark tests of the resulting prototype are presented and discussed. Finally, recommendations for future work on this device regarding performance and accuracy enhancements are listed

## METHODOLOGY

### Array Signal Processing

To characterize multiple sound sources simultaneously, specific algorithms exist that allow to “map the spatial distribution of acoustic sources in terms of sound pressure level radiated towards a reference position” (Herold & Sarradj, 2017). Over the years, many such algorithms of varying accuracy and computational cost have been proposed and compared in terms of performance (Herold & Sarradj, 2017). The basis of most of these data processing algorithms is a technique called Beamforming.

In the setting shown in figure 1, sound sources are being analyzed by an array of  $N$  microphones. If the pressures of all sound sources present in the grid were known, assuming linear superposition on the contributions of all sound sources, the sound pressure measured at a microphone  $n$  at an instant  $t$  could be calculated as:

$$p_n(t) = \sum_m a_{mn} q_m(t - \Delta\tau_{mn}) \quad (1)$$

Where  $\Delta\tau_{mn}$  is the time required for sound to travel from source  $m$  to microphone  $n$ ,  $q_m$  is the pressure of sound source  $m$ , in this case evaluated at an instant  $t - \Delta\tau_{mn}$ , and  $a_{mn}$  reflects the change in magnitude that the signal will suffer because of the distance between source  $m$  and microphone  $n$ .

However, when generating acoustic maps, the number and location of sound sources is generally not known. This can be tackled by partitioning the plane of study into equally spaced control points and then calculating the pressures at these specific points on the grid, given the measurements of an array of microphones. In other words, the inverse problem of that addressed by equation 1 must be solved.

The pressure at a source  $m$  in the grid can be calculated by a “weighted sum of delayed and attenuated microphone signals” (Sarradj & Herold, 2017):

$$p_m(t) = \sum_n h_{mn} p_n(t + \Delta t_{mn}) \quad (2)$$

Where  $h_{mn}$  accounts for the magnitude change because of the distance traveled by the signal from source  $m$  to microphone  $n$  and  $\Delta t_{mn}$  is the time required for sound to travel from source  $m$  to microphone  $n$ . Spatial filtering results from choosing  $h_{mn}$  and  $\Delta t_{mn}$  in a way that the calculated output for  $p_m$  contains only the signal from source  $m$ , and signals from other sources are suppressed as much as possible. This approach is known as Delay-and-Sum beamforming (Sarradj & Herold, 2017).

The procedure to calculate the filter coefficients  $h_{mn}$  and  $\Delta t_{mn}$  from  $a_{mn}$  and  $\Delta \tau_{mn}$  is shown in (Sarradj, 2012). The calculated pressures for all points can then be represented at once with a contour plot and placed on top of a digital image taken separately with a camera, to achieve the desired acoustic map. A hypothetical grid is shown in Figure 1.

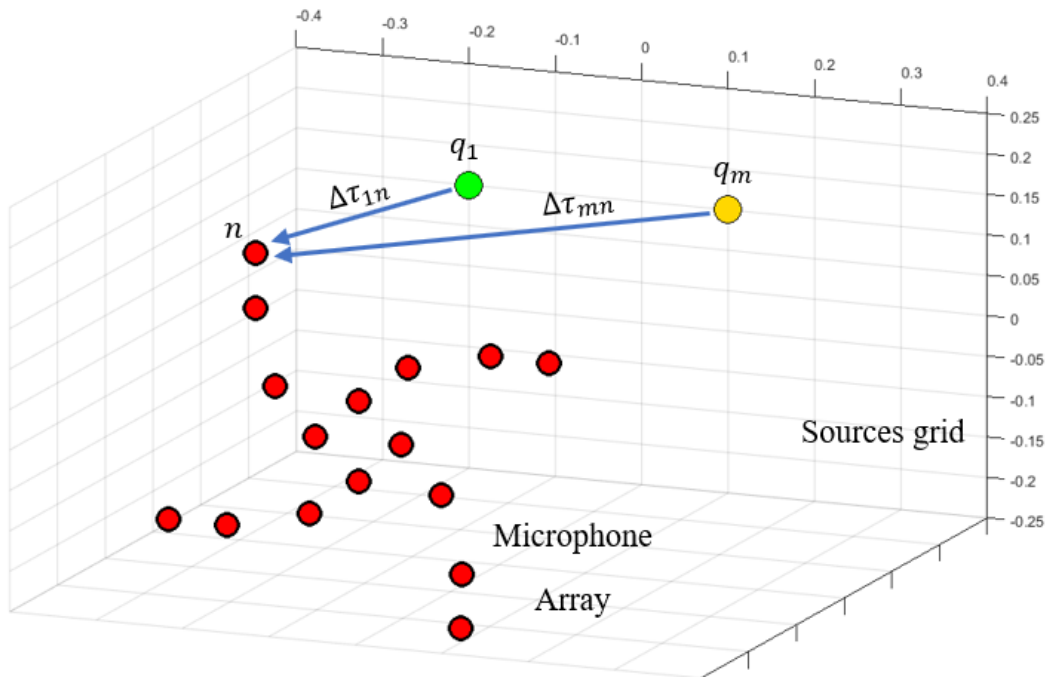


Figure 1. Working principle of beamforming.

## Microphone Array Design

Desirable features of microphone arrays include a wide dynamic range, high spatial resolution, and minimum artifacts/systematic errors (Herold & Sarradj, 2017). Microphone placement is a major design concern because it affects the working frequency range of the array (Le, Thomas, & Poisson, 2016), its ability to reject sources that it is not focused on, i.e. the Maximum Sidelobe Levels (Prime & Doolan, 2013), and its ability to distinguish sources from one another (a.k.a. resolution) (Aldeman & Raman, 2018). A key issue that needs to be avoided is spatial aliasing, which occurs when the intra-sensor spacing is not adequate for the wavelength being measured, yielding ‘ghost sources’ in the resulting acoustic map (Chiariotti, Martarelli, & Castellini, 2019).

To reduce this, spatial sampling based on the Nyquist rate could be implemented, i.e. arranging the microphones so that the distance between any two of them does not exceed one-half wavelength (Chiariotti et al., 2019). However, this is impractical for shorter wavelengths, since the number of required microphones would be considerable if large areas were to be covered (Chiariotti et. al., 2019).

An alternative to reduce spatial aliasing is to use arrays with almost unique intra-sensor spacings, also known as non-redundant or a-periodic arrays. These could be sparse, random or spiral, and although they may be more challenging to build than regularly shaped arrays, e.g. circular, lattice, or cross-shaped, they can drastically reduce spatial aliasing using relatively fewer microphones (Chiariotti et. al., 2019).

Sparse arrays result from arbitrarily removing microphones from a regular array. However, full removal of systematic patterns is not guaranteed, and the spatial aliasing problem could still arise. Random arrays do guarantee non-redundancy and virtual elimination of spatial aliasing problems. However, to achieve acceptable performance in terms of Minimum Side

Lobes, more microphones are needed than with other arrays per unit area, and to ensure an optimal placement, more sophisticated optimization methods are required.

Spiral arrays also guarantee zero-redundancy and out of the three types of a-periodic arrays mentioned, spiral arrays have been proven to yield the best compromise between number of sensors and reduction of unwanted effects (Chiariotti et. al., 2019).

A comparison of six spiral arrangements for beamforming systems was made by Prime and Doolan. The study included Archimidean, Dougherty log, Arcondoulis, Multi-arm and underbrink spirals (Prime & Doolan, 2013). Each array comprised 63 microphones and had an aperture of 1 meter. The criteria for comparison were the resolution normalized with respect to wavelength and the Minimum Sidelobe Levels (MSL), calculated at the “one-third octave band centre frequencies from 1 to 31.5 kHz” (Prime & Doolan, 2013).

It was concluded that the underbrink spiral arrangement yielded the best performance both in resolution and MSL. Hence, for this prototype, an underbrink spiral scheme (fig. 1) was selected for the arrangement of the microphones, using the equations provided.

For an underbrink spiral of  $N_a$  spiral arms,  $N_m$  microphones per arm, with a maximum radius  $r_{max}$ , a minimum radius  $r_o$ , and a spiral angle  $\nu$ , the distances of the microphones to the center of the array are given by the equations below (Prime & Doolan, 2013):

$$r_{m,1} = r_o, \quad m = 1:N_a \quad (3)$$

$$r_{m,n} = \sqrt{\frac{2n-3}{2N_m-3}} * r_{max}, \quad m = 1:N_a, \quad n = 1:N_m \quad (4)$$

And the angles are given by:

$$\theta_{m,n} = \frac{\ln\left(\frac{r_{m,n}}{r_o}\right)}{\cot(\nu)} + \frac{m-1}{N_a} * 2\pi, \quad m = 1:N_a, \quad n = 1:N_m \quad (5)$$

Figure 2 illustrates the microphone distributions used for the prototype, resulting from underbrink spiral designs for 16 microphones. A table with the exact locations and labels is presented under appendix A.

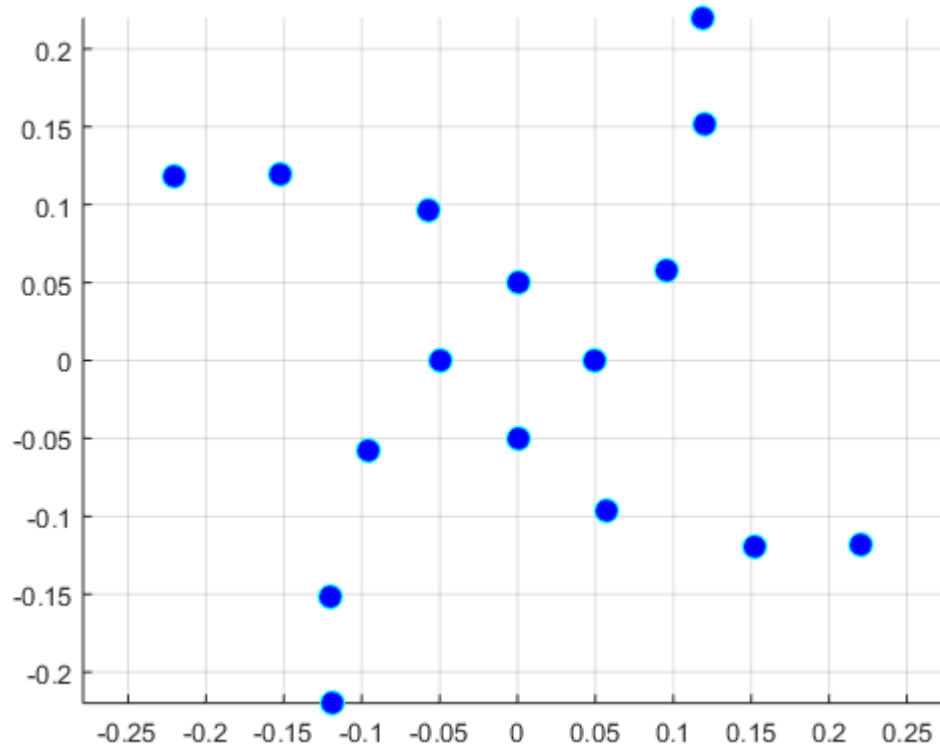


Figure 2. Underbrink spiral microphone array distribution,  $N_a = 4$ ,  $N_m = 4$ ,

$$v = \frac{3\pi}{16} \text{ rad}, r_{max} = 0.25, r_o/r_{max} = 0.2 .$$

## F Parameter

An indicator of array quality, the F parameter represents “the ratio between the actual number of unique vector spacing and the maximum one” (Chiariotti et al., 2019). For a perfectly irregular array, i.e. where the maximum intra-sensor spacings are maximized,  $F = 1$ .

Given  $M$  microphone positions ( each denoted by  $\vec{x}$  ), a matrix of dimensions  $M \times M$  known as the co-array matrix can be obtained by performing the following operation:

$$\vec{X} = \vec{x}_m - \vec{x}_n \quad ; \quad n = 1 \dots M \quad ; \quad m = 1 \dots M \quad (6)$$

This parameter is calculated from the following expression:

$$F = \frac{U}{U_{max}} = \frac{U}{M^2 - (M - 1)} \quad (7)$$

, where  $U$  is the number of unique elements in the co-array matrix previously defined.

The microphone geometry for the present prototype, an underbrink array with 16 microphones, yielded an  $F$  parameter of 0.274, a number that improves noticeably as more microphones are added to the array.

## Simulations

The acoular library allows for the generation of samples which can be used to simulate the behavior of microphone arrays. Hence, the arrangement of figure 2 was tested prior to construction by running an example presented in the acoular library literature (Herold & Sarradj, 2017). It consists of virtually locating three point-sources over a square area of 0.2 m by 0.2 m. The parameters for generation of these synthetic sources are summarized in the following table:



Table 1. Location and strength of three synthetic point sources with respect to the center of the array

Source	Location [m]	Rms sound pressure [Pa]
1	(-0.1, -0.1, 0.3)	1
2	(0.15, 0, 0.3)	0.7
3	(0, 0.1, 0.3)	0.5

The input data for each simulation was a file containing the generated samples for the corresponding number of channels, with a sampling frequency of 51200 Hz and a total sampling duration of 1 second.

The results obtained with the 16-microphone array (figure 2) are shown next. The plot shows the intensities and sound source locations computed for all the FFT lines within the 3 kHz third-octave band.

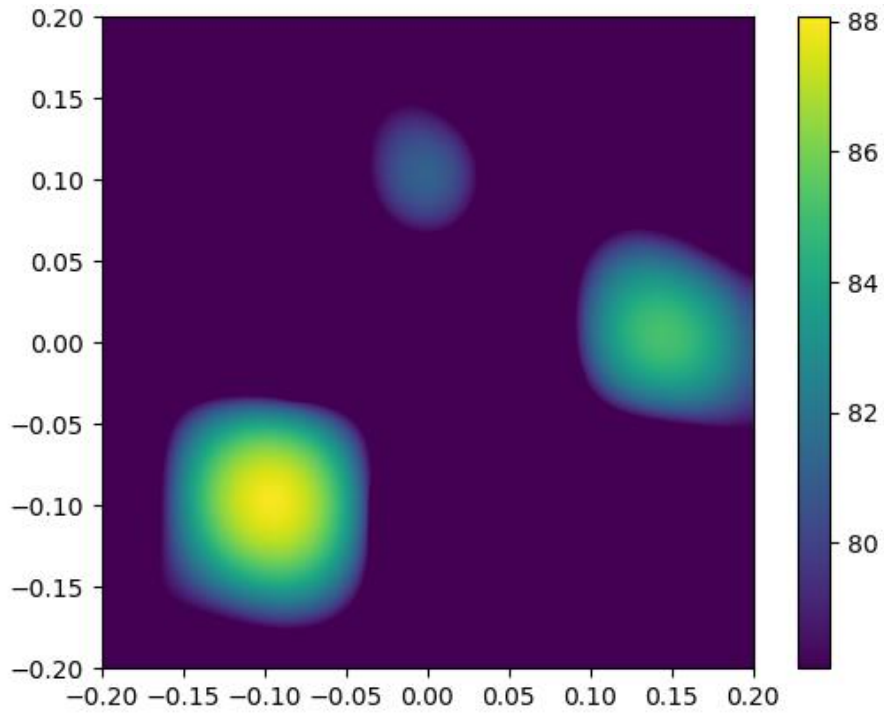


Figure 3. Acoustic map of three arbitrary point sources (3 kHz third-octave band, 16-microphone underbrink spiral array).

As the simulations show, the 16-microphone underbrink spiral array allows for successful location of the sources and calculation of sound pressure levels. However, due to the size of the array, it is relatively limited in terms of frequency range compared to a 64-microphone array. When analyzing the 10kHz third-octave band, the decrease in performance is evident, as ghost sources begin to appear:

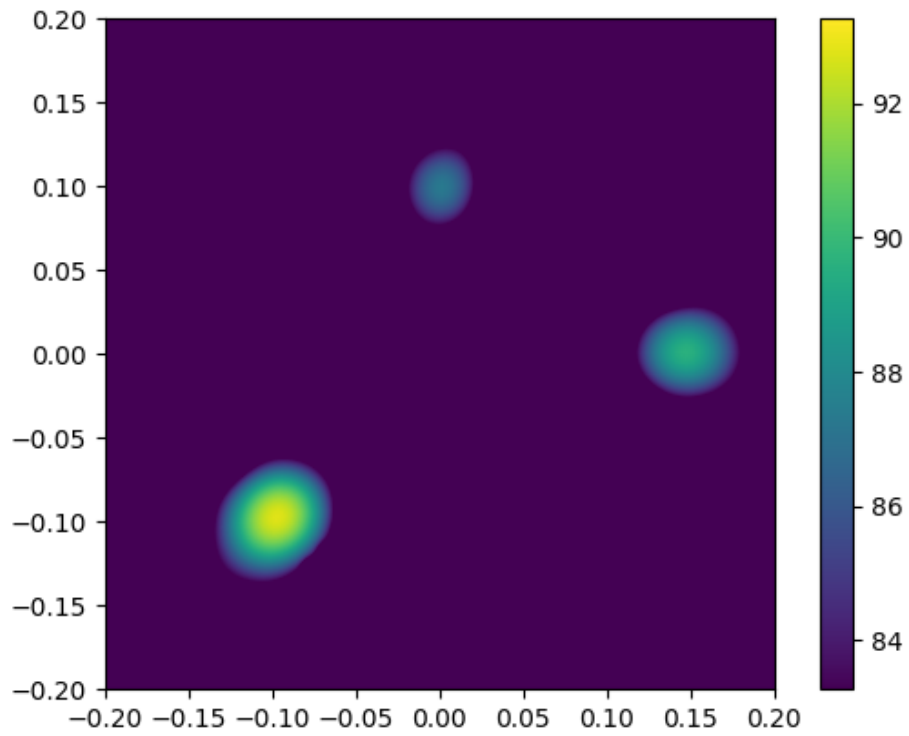


Figure 4. Acoustic map of three arbitrary point sources (10 kHz third-octave band, 64-microphone Underbrink spiral array).

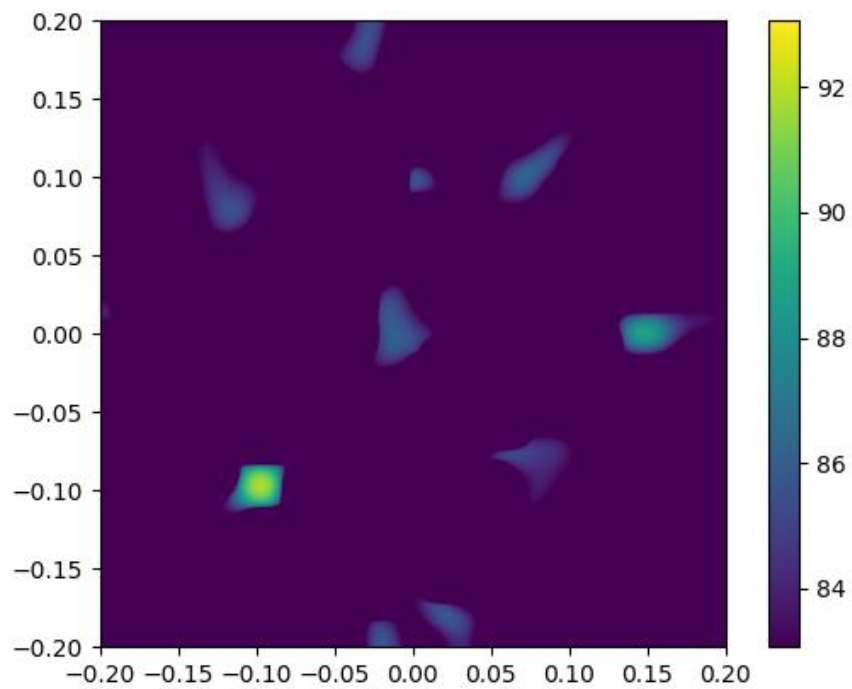


Figure 5. Acoustic map of three arbitrary point sources (10 kHz third-octave band, 16-microphone Underbrink spiral array).

## **Hardware and Software components**

### **Sensors**

A total of 16 Behringer ECM-8000 condenser microphones were used. These have a reported sensitivity of -70dB, which corresponds to 0.316 mV/Pa. An electric circuit and two 12 V DC power supplies (as well as 9V DC supply for the circuit itself) were used to provide the necessary voltage to the microphones and signal pre-amplification. The schematics of the circuit are presented under appendixes B & C.

### **Data acquisition**

A National Instruments cDAQ 9178 chassis along with four NI 9234 modules were used to record the signals of the 16 microphones simultaneously. Pictures were taken with a repurposed laptop webcam located in the center of the array. Both of these devices were connected via USB to a laptop where further processing would be carried out.

A virtual instrument (VI) was developed in LabView 2017 to handle connection with the hardware, trigger the measurement process and save the data to the disk in a hierarchical data format meant for high performance in scientific applications known as HDF5 (Sarradj & Herold, 2017).

### **Processing**

After the data was recorded and saved, it was processed with a Beamforming algorithm to produce the acoustic map. This task was performed by leveraging the Acoular library (version 19.08).

Calculating the acoustic maps is a CPU-intensive task. Hence, real-time characterization is not yet possible with the proposed software/hardware architecture. Given the nature of the beamforming algorithms, in which there are no data dependencies between the calculations done over the spatial grid points, these could be performed simultaneously on a massively parallel processor such as a modern general-purpose GPU. Belloch, et. al. explored this idea,

achieving real time sound localization in three dimensions with an spherical beamforming array and a GPU to handle the calculations (Belloch, Cobos, Gonzalez, & Quintana-Ortí, 2015). Therefore, further performance optimization could be achieved by re-writing the most resource-intensive routines to run on a GPU. This would constitute a valuable extension to the Acoular library; however, it is beyond the scope of this work.

### **User interface**

To allow the user to control the entire process from a single graphical user interface in LabView, without having to execute python scripts separately to run the computations, a client-server scheme was implemented.

The VI implemented in LabView communicates with a local python server through a socket connection under the protocol known as TCP/IP (Y. Daniel Liang, 2018). The purpose of this server is to listen to requests from the LabView client and invoke routines that will process the requested file(s) making use of the Acoular library. Upon completing the calculations, a figure pops up, with the resulting sound pressure level map, overlaid on a digital image of the studied object/space.

The end user gets presented with a single graphical interface (GUI) within LabView, in order to manage measurements, trigger signal processing and explore the results.



Figure # 6. Acoustic camera prototype built for this project.

## RESULTS

The following tests were conducted to verify the ability of the device to locate sound sources.

### Test set 1

The sound source was a tablet playing white noise, at 4 different positions and at 3 different distances from the camera: 0.3, 0.5 and 0.8 meters.



Figure # 7. Sound source set-up for test set # 1

At 0.3 meters, the SPL measured from the center of the array (using a cellphone as SPL meter), averaged over 15 seconds was 84.6 db.

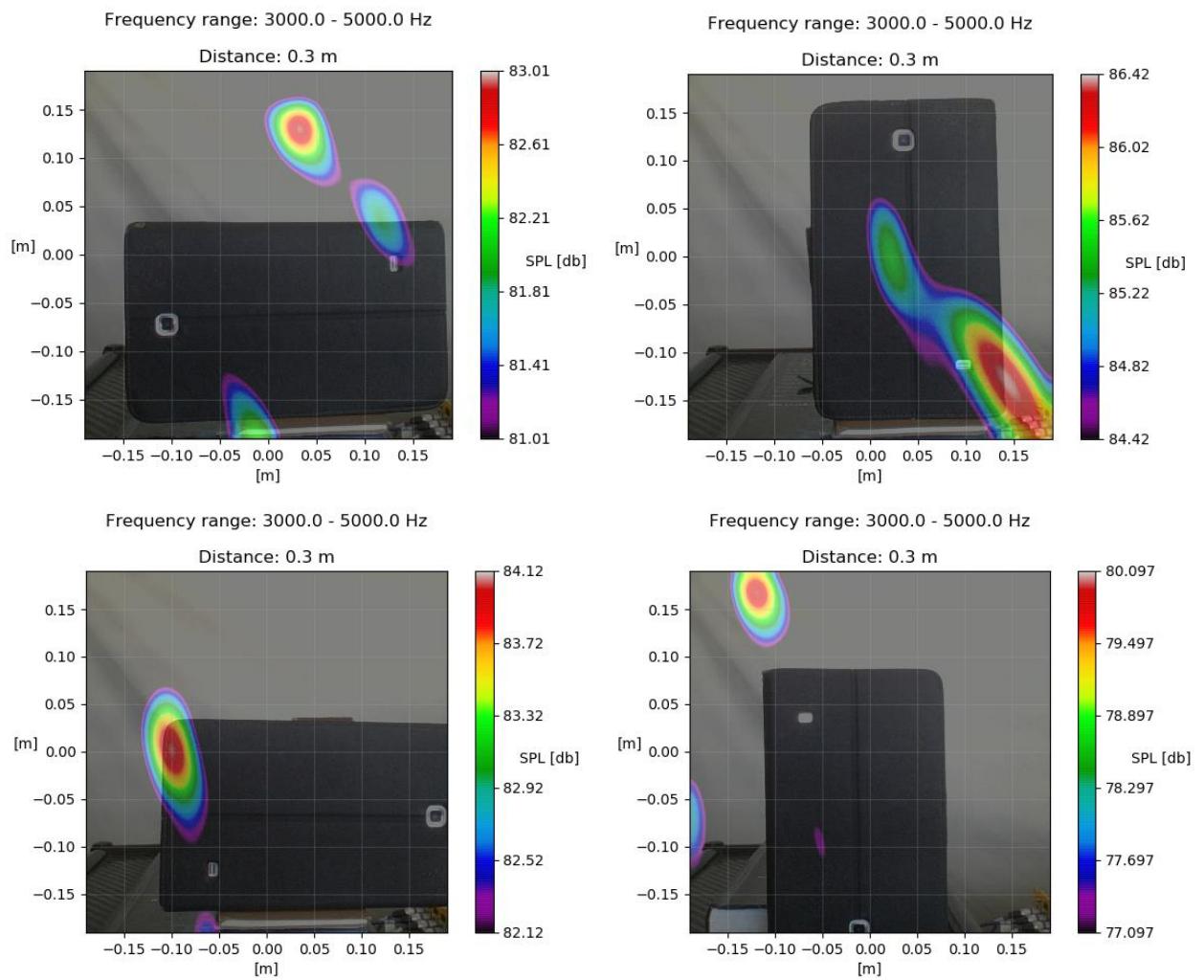


Figure # 8. Resulting acoustic maps for test set 1, at 0.3 m



At 0.5 meters, the SPL measured from the center of the array (using a cellphone as SPL meter), averaged over 15 seconds was 78.4 db.

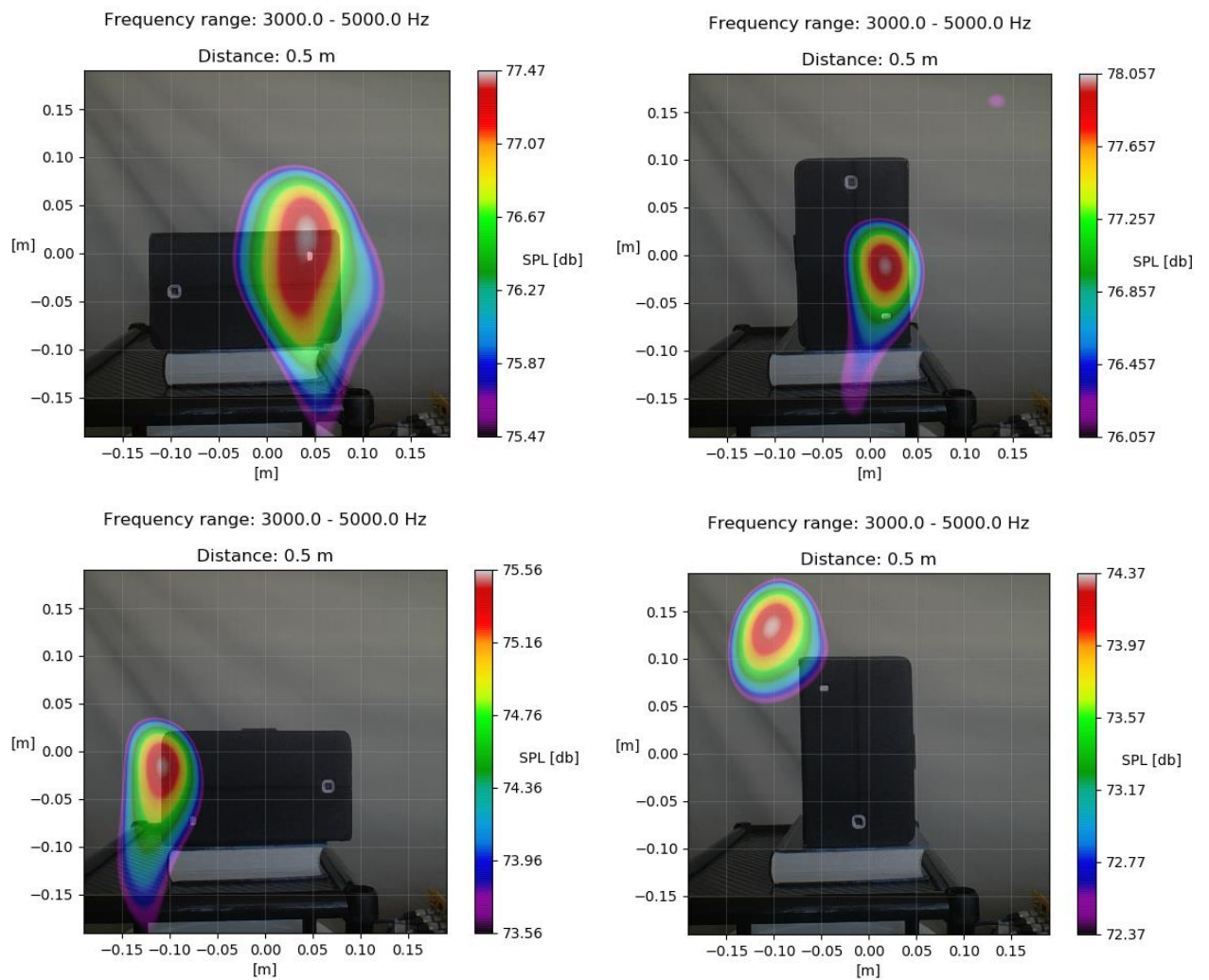


Figure # 9. Resulting acoustic maps for test set 1, at 0.5 m

At 0.8 meters, the SPL measured from the center of the array (using a cellphone as SPL meter), averaged over 15 seconds was 68.2 db.

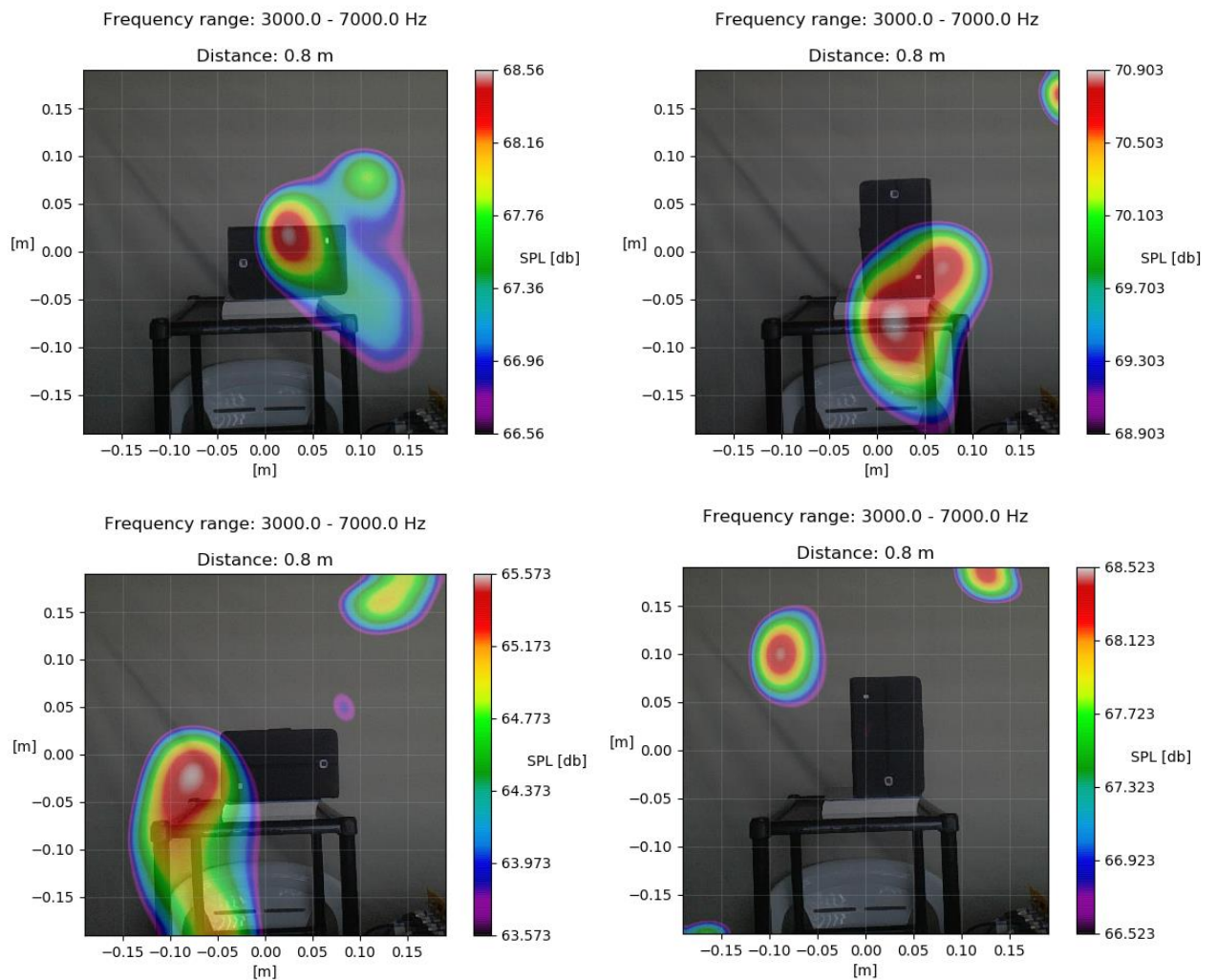


Figure # 10. Resulting acoustic maps for test set 1, at 0.8 m.

(Frequency range extended due to attenuations experienced in lower frequencies).

**Test set 2**

The sound sources were a tablet and a cellphone both playing white noise. Measurements were taken at a distance of 0.5 meters, with the tablet rotated to 4 different positions while the phone remained fixed.



Figure # 11. Sound source set-up for test set # 2

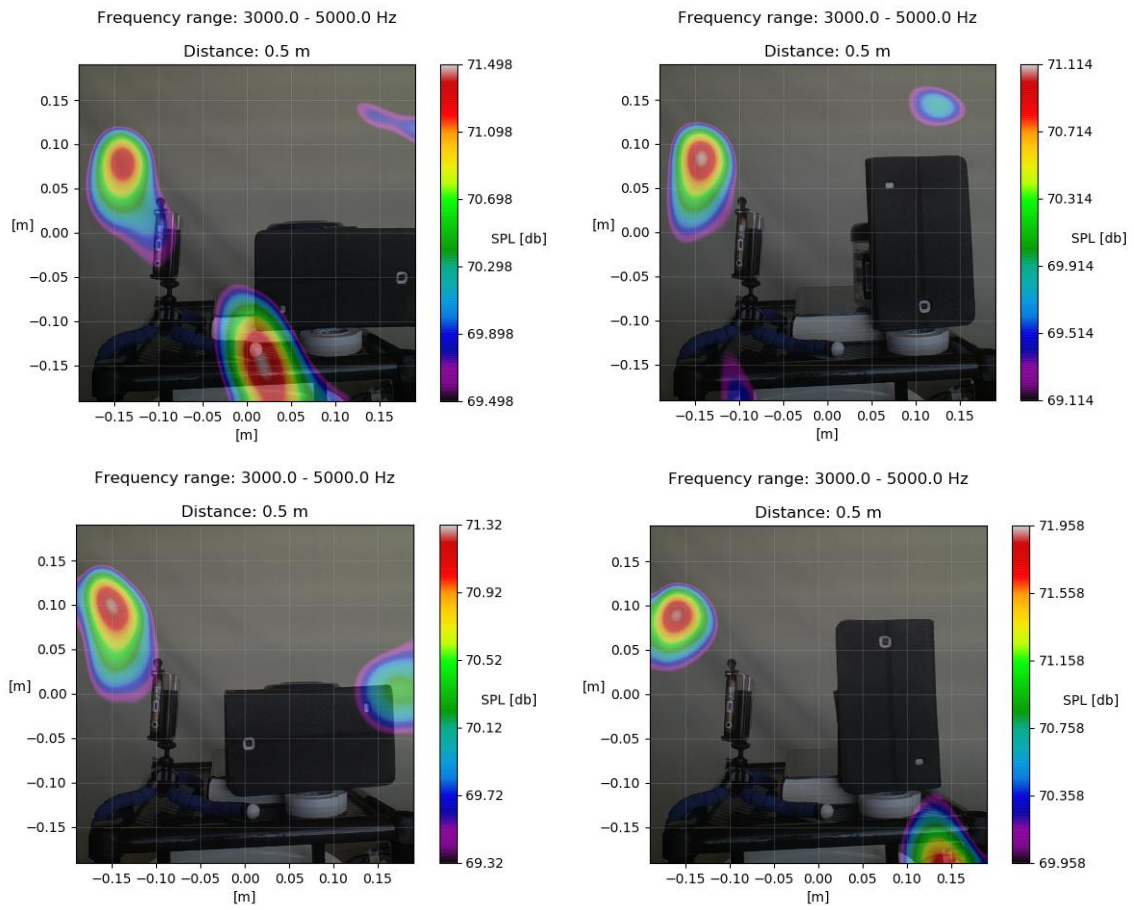


Figure # 12. Resulting acoustic maps for test set 2.

### Test set 3

The sound sources were again a tablet and a cellphone, but the tablet played white noise while the phone played a 4 kHz pure tone. Measurements were taken at a distance of 0.5 meters.

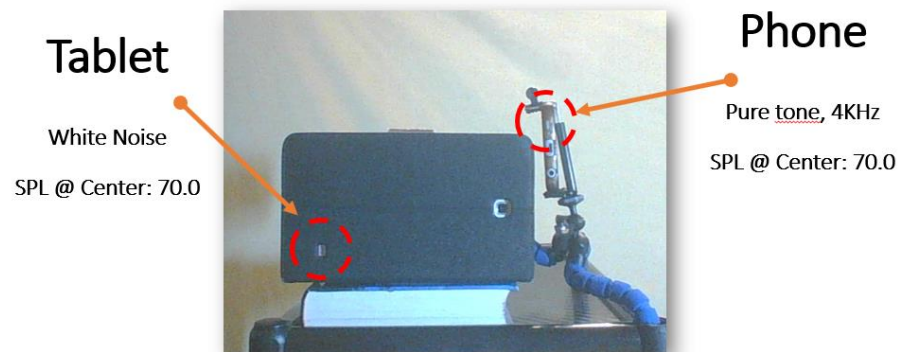


Figure # 13. Sound source set-up for test set # 3

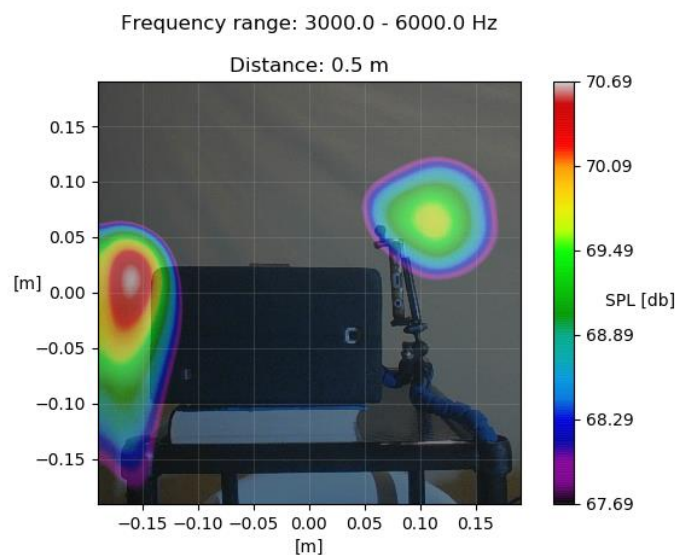


Figure # 14. Resulting acoustic map for test set # 3, from 3 kHz to 6 kHz

As expected, when analyzing a frequency range that includes both sound sources, they are both visible.

However, only the cellphone is visible when the band being analyzed is narrow enough to contain almost exclusively the signal emitted by it (pure tone at 4 kHz):

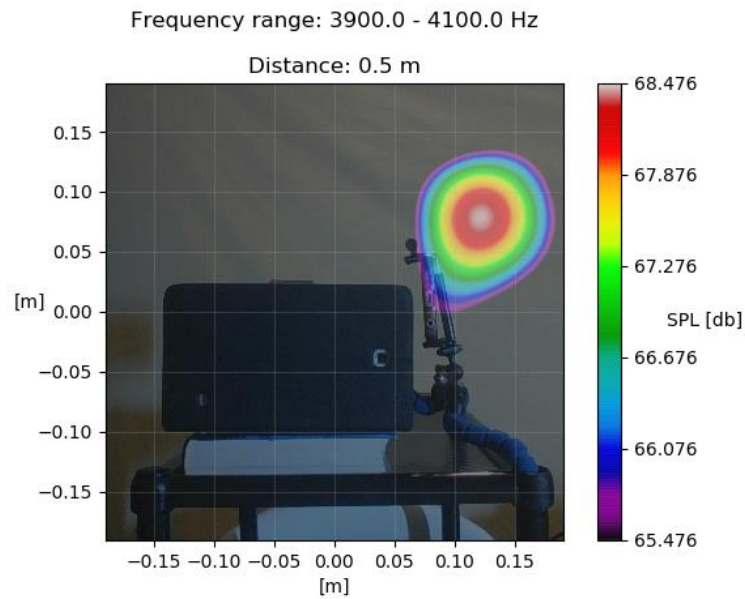


Figure # 15. Resulting acoustic map for test set # 3, from 3.9 kHz to 4.1 kHz

And only the tablet is visible when the frequency range being studied does not include 4 kHz:

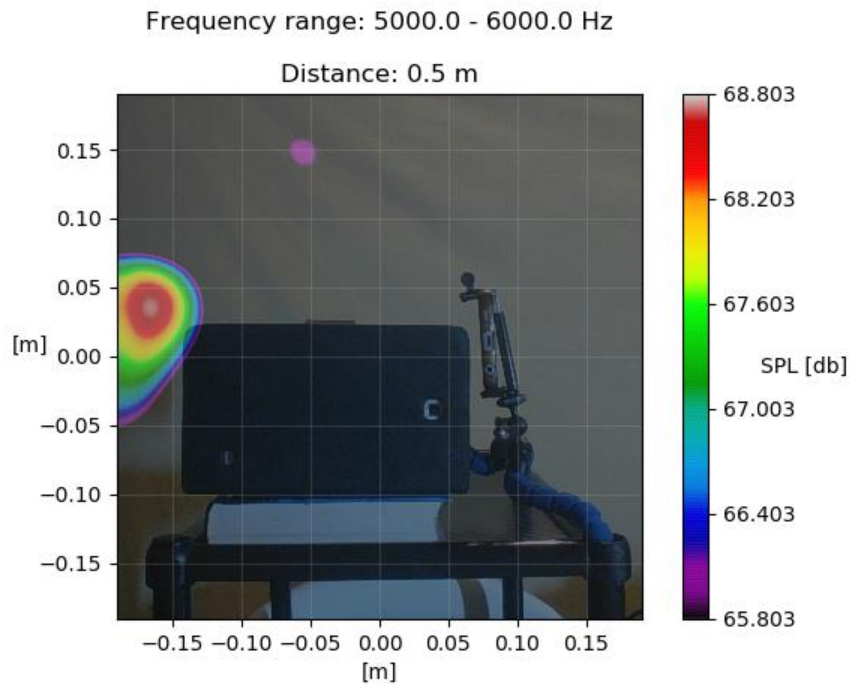
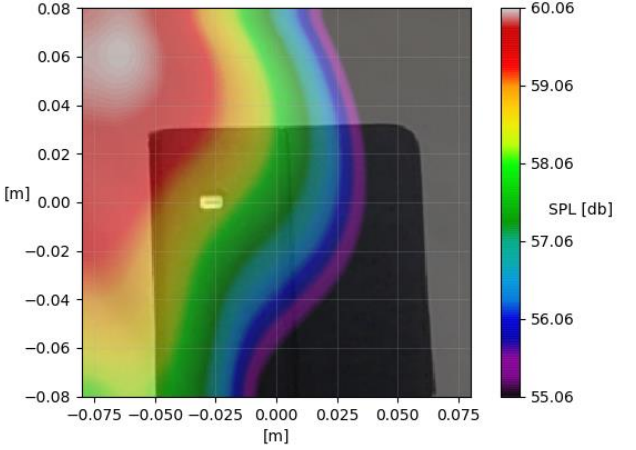
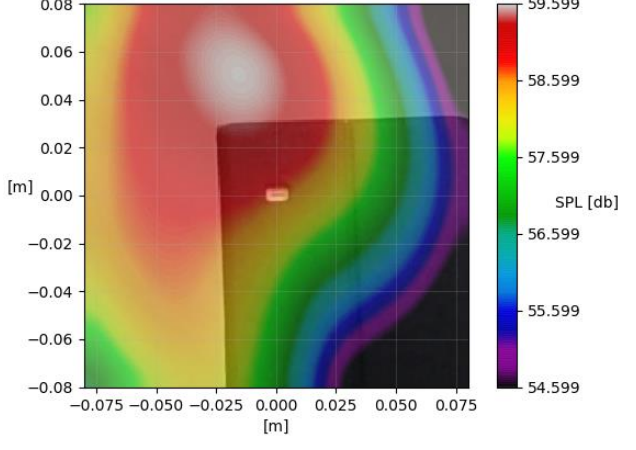
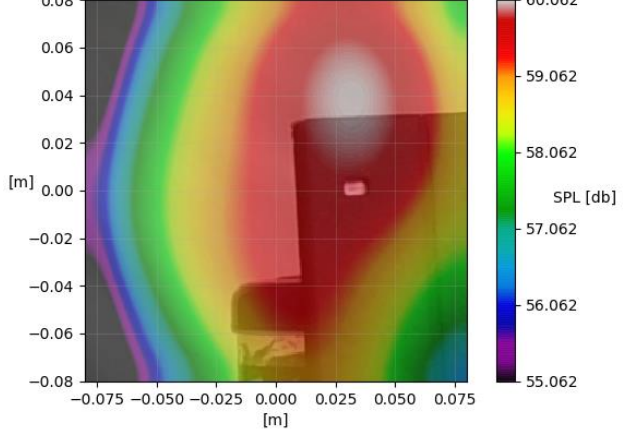


Figure # 16. Resulting acoustic map for test set # 3, from 5 kHz to 6 kHz

## DISCUSSION

The quantities of interest in acoustic maps are positions and intensities. Hence, there are two types of error relevant to these measurements. First, the localization error, which is calculated from the distance between the position of the maximum peak appearing in the acoustic map, and the position of the actual maximum, i.e. the positions of the speakers, estimated from the pictures. Second, the intensity error, calculated as the difference between the maximum SPL in the resulting acoustic map and the SPL measured from the center of the array by a single SPL meter. An additional set of tests with a single white-noise source at a distance of 0.5 meters was carried out. The frequency range studied is 3000 to 5000 Hz. The results are summarized in the following table.

Table 2. Localization and intensity errors (single sound source test, at 0.5 m from the array).

	Resulting Acoustic Map	Localization Error (cm)	SPL @ center (dB SPL)	Intensity Error (dB SPL)
Test 1	 <p>Acoustic map for Test 1. The x-axis ranges from -0.075 to 0.075 m, and the y-axis ranges from -0.08 to 0.08 m. A color scale on the right indicates SPL [db] from 55.06 to 60.06. The sound source is localized at approximately x = -0.025 m, y = 0.00 m.</p>	7.2	62	1.9
Test 2	 <p>Acoustic map for Test 2. The x-axis ranges from -0.075 to 0.075 m, and the y-axis ranges from -0.08 to 0.08 m. A color scale on the right indicates SPL [db] from 54.599 to 59.599. The sound source is localized at approximately x = 0.000 m, y = 0.00 m.</p>	5.4	64	4.4
Test 3	 <p>Acoustic map for Test 3. The x-axis ranges from -0.075 to 0.075 m, and the y-axis ranges from -0.08 to 0.08 m. A color scale on the right indicates SPL [db] from 55.062 to 60.062. The sound source is localized at approximately x = 0.025 m, y = 0.00 m.</p>	4.0	62	1.9



It is observed that the localization error tends to descend as the sound source is closer to the right of the array; this indicates an asymmetry in the response of the array. This issue needs to be addressed in future iterations of the prototype.

There are other aspects of the prototype in which there is room for improvement. Based on the observations, recommendations for future iterations of the device are:

- Increasing the F parameter to lower spatial aliasing effects, thus increasing the working frequency range of the device. As mentioned in the Microphone Array Design section, the F parameter for the array used in the current prototype is 0.274, whereas the ideal value is 1. This can be improved either by adding more microphones to the array or modifying parameters of the equation that generates the spiral positions (Prime & Doolan, 2013).
- Calibrating the microphones of the array against a professional-grade SPL meter. This would help reduce the intensity measurement error, since for this prototype the calibration procedure was carried out using a phone as reference SPL meter.
- Finally, exploring an alternative building method that guarantees the correct alignment of the camera in the center of the array, as well as rigid supports for the microphones, would help to reduce localization error, since slight deviations between the positions passed to the program and the actual positions of the microphones can greatly affect the results.

## CONCLUSIONS

Acoustic cameras provide the ability to characterize unknown sound sources in terms of location, intensity and spectrum. This can provide opportunities for unexplored applications in several fields, including machinery design and non-invasive diagnosis. With this study, an advance towards the development of an acoustic camera has been made, by developing a prototype that offers ease of use and a fast feedback loop.

The current prototype allows to locate and characterize sound sources, albeit in a narrow frequency range (2.8 to 6 kHz), and with a visible spatial error. From the tests performed, it was observed that this prototype works best at a distance between 0.5 and 0.8 meters of the analyzed object/scenario. Key aspects of the prototype with room for improvement regarding the working frequency range and accuracy in both sound pressure level measurement and sound source localization have been identified and insights have been provided for future iterations.

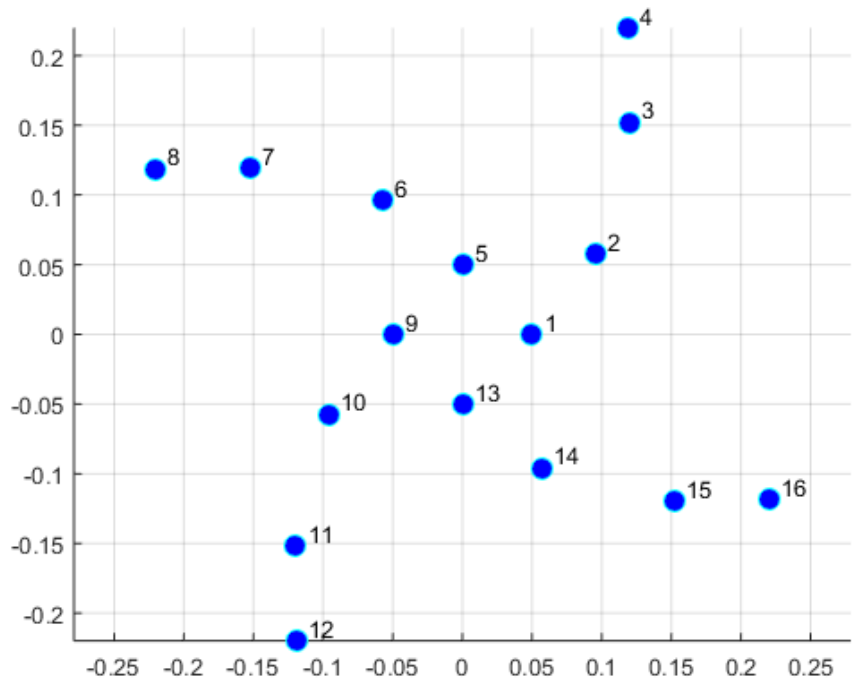
## REFERENCES

- Aldeman, M., & Raman, G. (2018). Effects of array scaling and advanced beamforming algorithms on the angular resolution of microphone array systems. *Applied Acoustics*, 132(November 2017), 58–81. <https://doi.org/10.1016/j.apacoust.2017.11.009>
- Belloch, J. A., Cobos, M., Gonzalez, A., & Quintana-Ortí, E. S. (2015). Real-time sound source localization on an embedded GPU using a spherical microphone array. *Procedia Computer Science*, 51(1), 201–210. <https://doi.org/10.1016/j.procs.2015.05.226>
- Chiariotti, P., Martarelli, M., & Castellini, P. (2019). Acoustic beamforming for noise source localization – Reviews, methodology and applications. *Mechanical Systems and Signal Processing*, 120, 422–448. <https://doi.org/10.1016/j.ymssp.2018.09.019>
- Döbler, D., & Heilmann, G. (2015). Perspectives of the Acoustic Camera. *Environmental Noise Control, The 2005 Congress and Exposition on Noise Control Engineering*, (AUGUST 2005), 1–9.
- Herold, G., & Sarradj, E. (2017). Performance analysis of microphone array methods. *Journal of Sound and Vibration*, 401, 152–168. <https://doi.org/10.1016/j.jsv.2017.04.030>
- Legg, M., & Bradley, S. (2014). Automatic 3D scanning surface generation for microphone array acoustic imaging. *Applied Acoustics*, 76, 230–237. <https://doi.org/10.1016/j.apacoust.2013.08.008>
- Orman, M., Rzeszucinski, P., & Pinto, C. T. (2014). *3D printed acoustic camera for electric motor diagnostics*. (Icaicte), 43–47. <https://doi.org/10.2991/icaicte-14.2014.10>
- Ortiz, N. M., Barré, S., & Vonrhein, B. (2015). The acoustic camera as a valid tool to gain additional information over traditional methods in architectural acoustics. *Energy Procedia*, 78, 122–127. <https://doi.org/10.1016/j.egypro.2015.11.126>
- Prime, Z., & Doolan, C. (2013). *A comparison of popular beamforming arrays*. (November), 1–7.

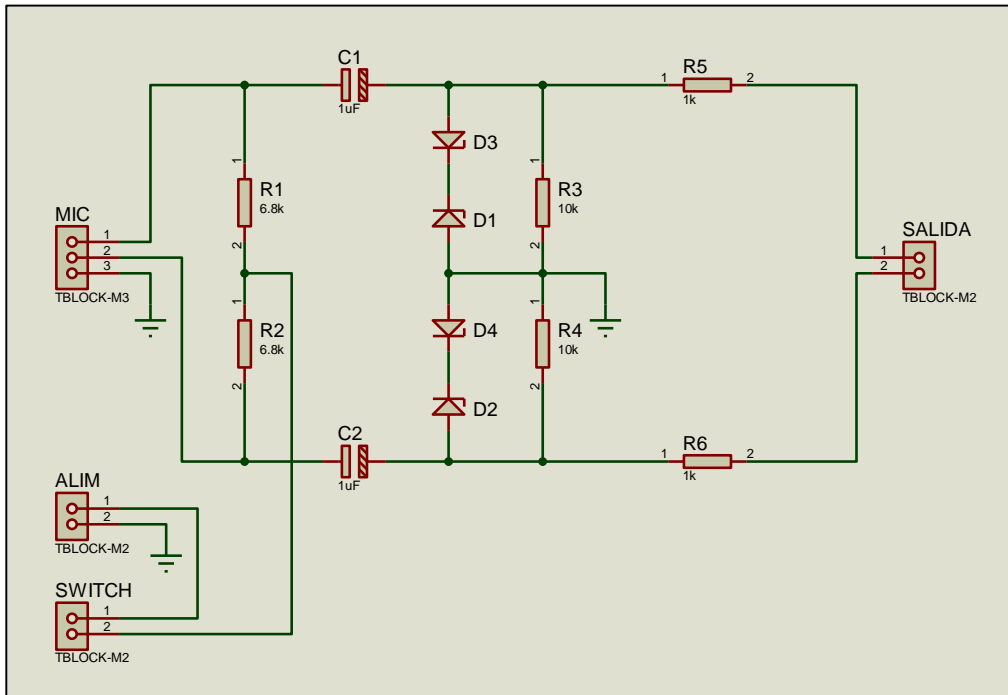
- Sarradj, E. (2012). *Three-Dimensional Acoustic Source Mapping with Different Beamforming Steering Vector Formulations*. 2012. <https://doi.org/10.1155/2012/292695>
- Sarradj, E., & Herold, G. (2017). A Python framework for microphone array data processing. *Applied Acoustics*, 116, 50–58. <https://doi.org/10.1016/j.apacoust.2016.09.015>
- Y. Daniel Liang. (2018). *Introduction to Java Programming and Data Structures, Comprehensive Version* (11th ed.). New York: Pearson.

**APPENDIX A: LAYOUT AND EXACT MICROPHONE POSITIONS IN THE  
ACOUSTIC CAMERA PROTOTYPE**

Mic	X (m)	Y (m)
	0.050	0.000
2	0.096	0.057
3	0.120	0.152
4	0.119	0.220
5	0.000	0.050
6	-0.057	0.096
7	-0.152	0.120
8	-0.220	0.119
9	-0.050	0.000
10	-0.096	-0.057
11	-0.120	-0.152
12	-0.119	-0.220
13	0.000	-0.050
14	0.057	-0.096
15	0.152	-0.120
16	0.220	-0.119



## APPENDIX B: CIRCUIT SCHEMATIC FOR THE MICROPHONE POWER SUPPLY STAGE



## APPENDIX C: CIRCUIT SCHEMATIC FOR THE MICROPHONE PRE-AMPLIFICATION STAGE.

